FEDSM2022-87690

COMPUTATIONAL MODELING AND HYDRODYNAMIC ANALYSIS OF FISH SCHOOLS IN THREE-DIMENSIONAL ARRANGEMENTS

Yu Pan, Wei Zhang, Haibo Dong

Department of Mechanical and Aerospace Engineering, University of Virginia Charlottesville, VA, USA

ABSTRACT

In this work, numerical simulations are employed to study hydrodynamic interactions in trout-like three-dimensional(3D) fish bodies arranged in vertical and horizontal planes. The fish body is modeled on a juvenile rainbow trout (Oncorhynchus mykiss) and is imposed on a traveling wave to mimic trout swimming. Three typical minimal schools are studied, including the in-line, the side-by-side, and the vertical school. A sharp interface immersed-boundary-based incompressible Navier-Strokes flow solver is then used to quantitively simulate the resulting flow and hydrodynamic performance of the schools. The results show that the hydrodynamic efficiency of the leading fish in the in-line school increases by 5.28%, and the thrust production and efficiency of the side-by-side school are enhanced by 2.28% and 3.86%, respectively. Besides, the thrust production of the vertical school increases by 21.6%. The results suggest great potential in exploiting the hydrodynamic benefits in fish schools arranged in three-dimensional space.

Keywords: immersed boundary method, fish school, swimming, three-dimension, spatial arrangement.

NOMENCLATURE

λ	wavelength of the traveling wave				
T	period of the traveling wave				
u_i	velocity component				
p	pressure				
ν	kinematic viscosity				
U_{∞}	incoming flow velocity				
ρ	fluid density				
Re	Reynold number				
St	Strouhal number				
V	vertical spacing				
S	streamwise spacing				
D	lateral spacing				
L	body length				
f	tail-beat frequency				

\boldsymbol{A}	tip-to-tip amplitude of the undulation
C_T	thrust coefficient
C_D	drag coefficient
C_{PW}	power coefficient
η	hydrodynamic efficiency

1. INTRODUCTION

Fish school, as one of the most spectacular collective behaviors in nature, has attracted much attention in recent years. Fish may form a school because of various reasons, including mating[1], protecting[2], and foraging[3]. Numerous studies have shown that hydrodynamics is one of the most essential mechanisms governing the organization of fish schools[4, 5]. Weihs, using a two-dimensional (2D) model, theoretically demonstrated that fishes gained energetic benefits by forming a diamond configuration in the horizontal plane through vortex interaction and channeling effect[6].

Weihs's work implies that the spatial arrangement of fish is one of the most important factors determining the hydrodynamic performance of a school. Later on, numerous experimental and computational studies were conducted to investigate the effects of spatial arrangement on hydrodynamics. Recently, through two-pitching-foil experiments, Boschitsch et al.[7] found that in an in-line configuration, the thrust and propulsive efficiency of the downstream foil is improved by 50%, respectively, when the distance between foils is around 1.2 chord length. Besides, Dewey et al.[8] found that the efficiency of two side-by-side pitching foils is enhanced by 35% when the lateral distance is 0.5 chord length in the experiments. More recently, Kurt et al.[9] experimentally and theoretically studied the hydrodynamics of two pitching foils in a staggered formation and reported that when the streamwise spacing is 0.75 chord length, and the lateral spacing is 0.4 chord length, the follower produces 80% more thrust than in isolation. The hydrodynamic analysis of minimal schools demonstrates the performance of swimmers can be improved by varying the spatial arrangement of a school.

The hydrodynamic performance of schools involving more swimmers has been investigated. Hemelrijk et al.[10] using a multi-particle collision dynamics model proved that fish swimming in a diamond school achieve higher efficiency than swimming in solitary. Besides, through 2D numerical simulations, Pan and Dong [11] showed that the thrust production of tailing fish in a high-density diamond school, in which the lateral distance is 0.4 body length (BL), is 77.3% higher than that of a single fish, and the propulsive efficiency is enhanced by 41.4%. Furthermore, some researchers[12, 13] employed 3D fish models to investigate hydrodynamic interactions in a school constrained in a 2D plane.

In nature, however, not only the fish models are threedimensional, but the formation of a fish school is also threedimensional. Thus, more specific research should be conducted on hydrodynamic interactions in fish schools arranged in threedimensional space.

The fish body in this work is modeled on a juvenile rainbow trout (Oncorhynchus mykiss). A traveling wave motion that resembles the observations of carangiform swimming is employed to drive the undulatory motion of the body. Then, three two-fish schools are arranged in the in-line, side-by-side, and vertical configurations, respectively, and simulated in a sharpinterface immersed-boundary-method (IBM) based incompressible flow solver. The swimming performance of these schools is reported and compared. The corresponding vortex structures are also presented and analyzed to reveal the underlying mechanisms. An outline of this paper is as follows. Section 2 describes a trout-like fish model and its kinematics, the definition of three arrangements, the numerical methods, and the simulation setup. A detailed discussion about the hydrodynamic performance and the vortex structures of the schools is presented in Sec. 3. Finally, conclusions are provided.

METHODOLOGY

2.1 Trout-like fish model. undulatory motion kinematics, and school arrangements

The trout-like fish model is from the reconstruction of live juvenile trout experiments in Autodesk Maya (Autodesk Inc.). To capture the main characteristics of fish school swimming while keeping the problem complexity manageable, we keep the trunk (TK) and the caudal fin (CF) of the fish but remove other fins on the body such as the pelvic, dorsal, and pectoral fins. The body length of the fish is L normalized as one, and the body is straight at rest. By oscillating the mid-line in the transverse direction, the body propels itself at a certain speed U_{∞} . Instead of directly employing the kinematics recorded in the experiments, a traveling wave motion[14] is imposed on the body, and some parameters are controlled to mimic the undulating motion of trout. The traveling equations are as follows

$$x(z,t) = A(z) \cdot \sin\left(\frac{2\pi}{\lambda}z - \frac{2\pi}{T}t\right),\tag{1}$$

$$A(z) = a_2 z^2 + a_1 z + a_0,\tag{2}$$

$$A(z) = a_2 z^2 + a_1 z + a_0, (2)$$

where x and z are the variables to denote the position of points on the trout body during the undulating motion, λ and T

indicate the wavelength and the period of the traveling wave, respectively. A(z) represents the amplitude envelope of the lateral motion of a point on the body, and a_i s are the coefficients of the quadratic polynomial function. In this work, $\lambda = 1.03$, T = 1, and the coefficients $a_0 = 0.011$, $a_1 = -0.105$ and $a_2 =$ 0.206. Figure 1 presents the definition of the midline of the trout model, the amplitude envelope of the trout motion, and a sequence of midlines during one tail-beat cycle.

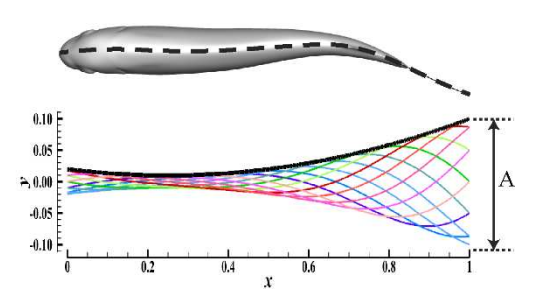


FIGURE 1: DEFINITION OF THE MIDLINE OF THE TROUT MODEL, TRAVELING WAVE AMPLITUDE (BLACK LINE), AND MIDLINES OF THE TROUT MODEL DURING UNDULATORY MOTION (COLORFUL LINES).

After obtaining the kinematics of a single fish, the minimal fish schools are formed by two trout fish arranged in the in-line, side-by-side, and vertical arrangements, respectively, as shown in Fig. 2. In this work, we use A1 to denote the in-line configuration, A2 to represent the side-by-side configuration, and A3 the vertical configuration. In addition, in Fig. 2, S is the streamwise spacing in A1, D is the lateral spacing in A2 and V is the vertical distance between fish 1 and fish 2 in A3. In this work, S = 1.2, D = 0.35, and V = 0.25.

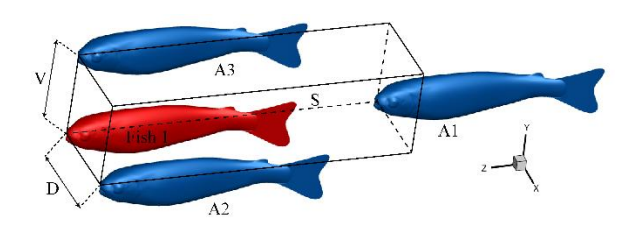


FIGURE 2: SCHEMATIC OF THREE MINIMAL SCHOOLS AND DEFINITIONS OF QUANTITIES DESCRIBING THE SPATIAL **ARRANGEMENTS**

2.2 Numerical methods and case setup

The governing equations considered in this work are 3-D unsteady Navier-Stokes equations for a viscous incompressible flow, written in an indicial form as,

$$\frac{\partial u_i}{\partial x_i} = 0, \quad \frac{\partial u_i}{\partial t} + \frac{\partial u_i u_j}{\partial x_j} = -\frac{1}{\rho} \frac{\partial p}{\partial x_i} + \nu \frac{\partial^2 u_i}{\partial x_j \partial x_j}, \tag{3}$$

where the u_i are the velocity components, p is the pressure, and ρ and ν denote the fluid density and the kinematic viscosity, respectively.

A finite-difference Cartesian-grid sharp-interface immersed boundary method[15] is employed to solve the above equations.

In this method, the complex moving boundaries are conducted on stationary Cartesian grids, and the Navier-Stokes equations are discretized using a cell-centered, collocated arrangement of the primitive variables. A fractional step method is employed to obtain second-order accuracy in time for these unsteady equations. A second-order Adams-Bashforth scheme is employed for the convection terms, while the diffusion terms are discretized using an implicit Crank-Nicolson scheme. This method has been successfully applied to simulate biological fish swimming[16], fish-like swimming[11, 17], and other flapping propulsions[18-21]. In this work, the adaptive mesh refinement (AMR) technique has been used to speed up simulations. More details about the AMR technique in the solver can be found in Ref.[22].

Figure 3 shows a schematic of the nonuniform Cartesian grid employed in the paper. In this work, three AMR layers have been used, and there are four AMR blocks in total. In the base layer, the domain size is $10L \times 6L \times 15L$ with grid points of $177 \times 113 \times 337$ (approximate 6.74 million) in total. The minimum grid spacing at the third layer is $\Delta_{min} = 3.57 \times 10^{-3}L$, which has proven fine enough to get the grid-independent results[16]. A constant velocity incoming flow boundary condition is set at the upstream boundary. At all the lateral boundaries, the zero-gradient boundary condition is applied. A homogeneous Neumann boundary condition is used for the pressure at all boundaries.

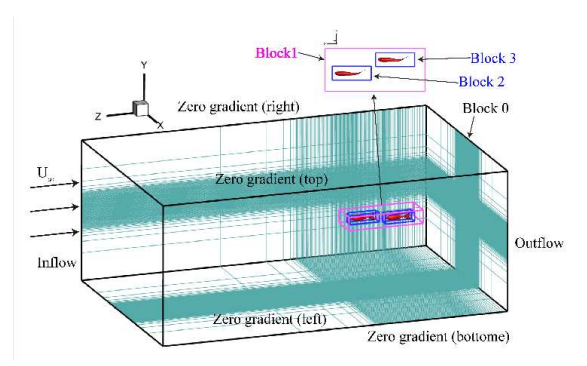


FIGURE 3: SCHEMATIC OF THE COMPUTATIONAL MESH AND BOUNDARY CONDITIONS.

Two important non-dimensional parameters, Reynolds number (Re) and Strouhal number (St), are used to describe the hydrodynamics and flow characteristics of fish-like swimming. The Re is defined as Re = $U_{\infty}L/\nu$, and the St is defined as St = fA/U_{∞} , where f is the tail-beat frequency; A is the peak-to-peak amplitude of the CF. Using a similar method in Ref. [11], the steady-swimming condition for a single trout can be obtained. And under the condition, Re = 5430 and St = 0.41.

The forces on the fish body are computed through direct integration of the surface pressure and shear. The thrust and drag are presented as non-dimensional coefficients, C_T and C_D . They are defined as $C_T = F_T/0.5\rho U_\infty^2 A_{CF}$ and $C_D = -F_D/0.5\rho U_\infty^2 A_{CF}$, where A_{CF} is the area of the CF. The hydrodynamic power is normalized as $C_{PW} = P/0.5\rho U_\infty^3 A_{CF}$. Accordingly, the cycle-average force coefficients and power

coefficient are denoted by $\overline{C_T}$, $\overline{C_D}$ and $\overline{C_{PW}}$, respectively. The hydrodynamic efficiency η is represented as the thrust-to-power ratio, $\eta = \overline{C_T}/\overline{C_{PW}}$.

3. RESULTS AND DISCUSSION

In this section, we first present the time history of drag on the TK, thrust on the CF, and the associated power coefficients of each fish in schools and compare them with that of a solitary trout. Then, the cycle-averaged forces, power coefficient, and swimming efficiency are calculated to measure and analyze each school's performance. Finally, visualized vortex structures, velocity field, and surface pressure differences are presented to reveal the underlying hydrodynamic mechanisms in each school.

3.1 Hydrodynamic performance of fish in schools

Figure 3 presents the time history of drag generated by the TK of fish 1 and fish 2 in each school and the associated power consumption on the TK. The drag and power consumption of the single-fish TK are also shown. In the in-line school, the drag on fish 1 is smaller than that on a single fish. At t=4.34T, the peaks of C_D of each fish reach, and $C_{D,max}^{A1-1}=0.300 < C_{D,max}^{single}=0.304$. Whereas, in the side-by-side school and vertical school, the drag on fish 1 increases. Correspondingly, the TK of fish 1 in the vertical school consumes the highest power. At t=4.72T, $C_{PW-TK}^{A3-1}=0.463$ is larger than that of the single fish $C_{PW-TK}^{single}=0.448$.

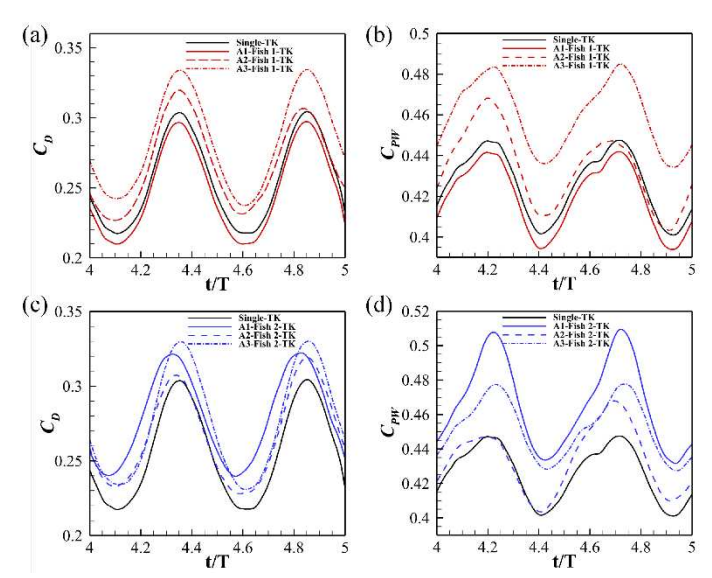


FIGURE 4: (A) DRAG COEFFICIENTS OF FISH 1 TK IN THREE SCHOOLS AND A SOLITARY FISH TK DURING ONE TAIL-BEAT CYCLE, (B) POWER CONSUMPTION ON TK OF FISH 1 IN SCHOOLS AND THE SINGLE FISH, (C) DRAG COEFFICIENTS OF THE TK OF FISH 2 AND THE SINGLE FISH, (D) POWER CONSUMPTION ON THE TK OF FISH 2 AND THE SINGLE FISH.

In the in-line school, the drag and power consumption on the TK of fish 2 increases. For example, at t=4.35T, $C_D^{A1-2}=0.335$ is 10% larger than $C_D^{single}=0.304$, and when t=0.335

4.20T $C_{PW-TK}^{A1-2} = 0.470 > C_{PW-TK}^{single}$. Due to symmetry, fish 2 has the same performance as fish 1 in the side-by-side school. In the vertical school, even though the upper part and the bottom part of the body are not symmetrical, the performance of fish 2 is close to that of fish 1: the drag and the associated power consumption on the TK of the two fish increase.

Figure 4 presents the time history of thrust generated by the CF of fish 1 and fish 2 in schools and the associated power consumption. Similarly, the thrust and power consumption of the single fish CF are also shown. In Fig. 4, it can be seen that the performance of fish CF in three schools is very close to that of the single fish, except that C_T^{A2-1} and C_T^{A2-2} both slightly increase, while C_{PW}^{A2-1} and C_{PW}^{A2-2} decrease in the side-by-side school.

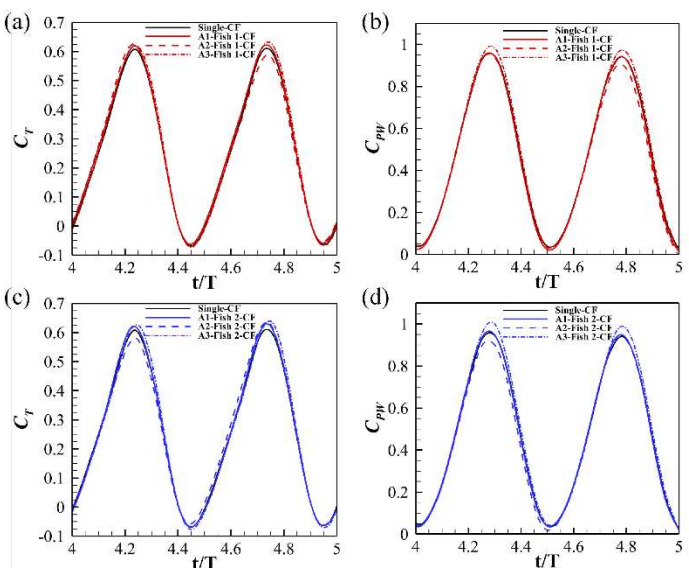


FIGURE 5: (A) THRUST COEFFICIENTS OF FISH 1 CF IN THREE SCHOOLS AND A SOLITARY FISH CF DURING ONE TAIL-BEAT CYCLE, (B) POWER CONSUMPTION ON CF OF FISH 1 AND THE SINGLE FISH, (C) THRUST COEFFICIENTS OF FISH 2 AND THE SINGLE FISH, (D) POWER CONSUMPTION ON CF OF FISH 2 AND THE SINGLE FISH.

TABLE 1. SUMMARY OF HYDRODYNAMIC PERFORMANCE OF A SINGLE TROUT

TK		CF		20	
$\overline{C_D}$	$\overline{C_{PW}}$	$\overline{\mathcal{C}_T}$	$\overline{C_{PW}}$	"	
-0.257	0.426	0.259	0.479	0.286	

The single trout's cycle-averaged performance and hydrodynamic efficiency are calculated and summarized in Table 1. The drag and thrust of the single fish presented in Table 1 proves that the steady swimming condition has been achieved. For comparison, the differences in performance between each fish in schools and the single fish are summarized in Table 2 in the percentage format.

In Table 2, it can be seen that the C_T of each fish is enhanced. In particular, the C_T of fish 1 and fish 2 in the vertical

school increase by 12.77% and 8.83%, respectively. Also, in the side-by-side school, the C_T of fish 1 is enhanced by 3.78%. However, except for fish 1 in the in-line school, C_D of all other fish increases by more than 4%. Specifically, C_D of fish 2 in the in-line school increases by 9.15%, which implies that the vortex flow shed by fish 1 in the in-line school is significantly detrimental to the performance of the trunk of fish 2. Besides, C_D of fish 1 and fish 2 in the vertical school increase by 15.12% and 13.63%, respectively, compared to a single trout. As for the hydrodynamic efficiency, the η of fish 1 in the in-line school is improved by 5.28%, while that of fish 2 reduces by 3.17%. The η of the side-by-side school and the vertical school increase by 3.86% and 1.72%, respectively.

TABLE 2. SUMMARY OF HYDRODYNAMIC PERFORMANCE DIFFERENCE OF EACH TROUT

Case		$\overline{C_T}$	$\overline{C_{PW}^{CF}}$	$\overline{C_D}$	$\overline{C_{PW}^{TK}}$	η
A1	Trout 1	3.78%	-1.40%	-2.82%	-1.46%	5.28%
	Trout 2	1.38%	0.42%	9.15%	9.51%	-3.17%
A2	Trout 1	1.00%	-3.17%	4.45%	1.81%	1.84%
	Trout 2	1.28%	-3.00%	4.46%	1.83%	2.02%
А3	Trout 1	12.77%	7.26%	15.12%	12.63%	2.71%
	Trout 2	8.83%	8.92%	13.63%	11.05%	-0.99%

3.2 Vortex wake analysis and Surface pressure

Due to thrust peaks being shown around t = 4.75T, we present the flow field of the single trout and schools at this time. The wake structures are visualized by the q-criterion[23]. Q = 4 and Q = 1.5 iso-surface values are chosen to identify the wake structures. At steady swimming, a trout sheds two lines of linked vortex rings to the downstream, and the vortex rings expand laterally in the horizontal plane, as shown in Fig. 5(a). Besides, the vortex rings are observed to stay stable in the vertical plane. Moreover, the velocity around the snout of the trout is lower than the incoming flow velocity. At the same time, a high-velocity zone exits in the middle part of the body and behind the tail.

By comparison, we find that, in the in-line school, the vortices shed by fish 1 interacts with the trunk of fish 2. The lowvelocity zone in front of fish 2 is reduced, and velocity around the middle part increases, as shown in Fig. 5(b), which results in the essential increase in drag on fish 2. Strong leading-edge vortices are generated on the caudal fins and shed downstream in the sides-by-side school. Thus, more thrust has been generated by the caudal fins. In addition, a channel is formed in the sideby-side school, and the velocity of the flow is high in the channel, which results in a higher drag and power consumption on the trunk. Finally, stronger leading-edge vortices are generated on the lower side caudal fin of fish 2 and the upper side caudal fin of fish 1 in the vertical school. Besides, the two sets of shedding vortex rings lean towards the center due to mutual interaction. Therefore, thrust production of the caudal fins is greatly enhanced. However, at the same time, high-velocity zones are

generated between fish 1 and fish 2. The high-velocity zone between the TKs increases the drag and power consumption.

Furthermore, we also present the surface pressure difference between fish in schools and the single fish in Fig. 7. There is a larger difference on the TK of fish 2 in the in-line school, while the pressure difference on the TK of fish 1 is slight. This implies a larger pressure difference due to the vortex interaction results in an increase in drag of fish 2 in the in-line school. Also, in other schools, the pressure difference on the trunk of each fish is higher than that of fish 1 in the in-line school. This suggests a higher drag on each fish in other schools. Besides, the larger pressure difference on the CFs explains the higher thrust production of each fish in these schools.

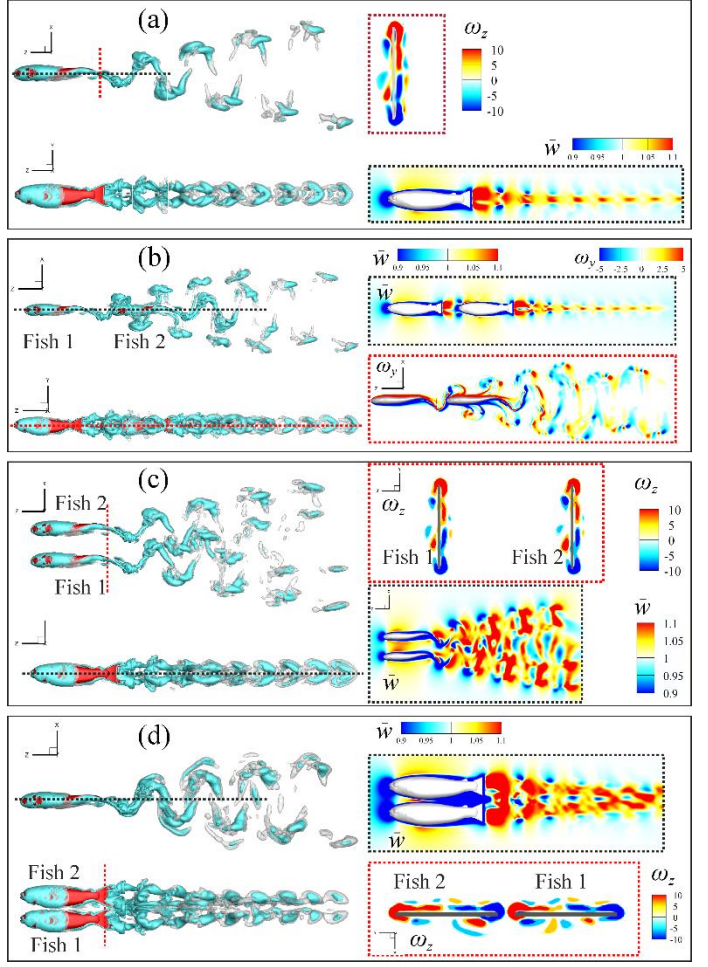


FIGURE 6: THREE-DIMENSION WAKE STRUCTURES, VORTICITY CONTOUR, AND NORMALIZED STREAMWISE VELOCITY CONTOUR ON DIFFERENT SLICES (A) A SOLITARY TROUT, (B) THE IN-LINE SCHOOL, (C) THE SIDE-BY-SIDE SCHOOL, (3) THE VERTICAL SCHOOL AT t=4.75T. THE POSITIONS OF SLICES ARE MARKED WITH RED, BLUE AND BLACK DOTTED LINES.

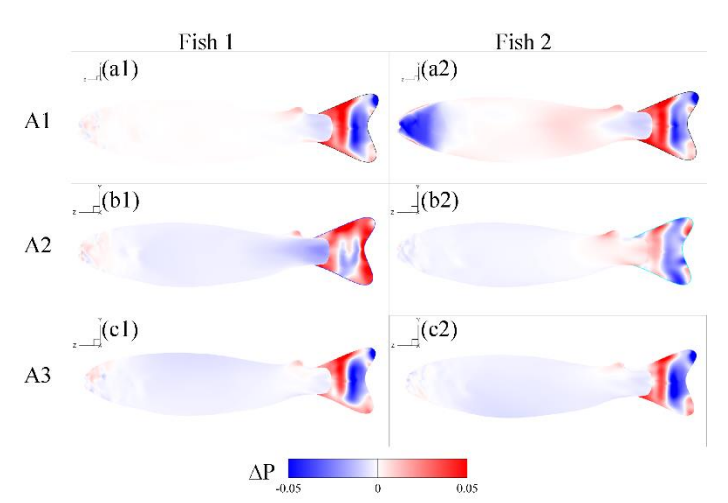


FIGURE 7: SURFACE PRESSURE DIFFERENCE BETWEEN A SOLITARY TROUT AND THE FISH IN (A) THE IN-LINE SCHOOL, (B) THE SIDE-BY-SIDE SCHOOL, AND (C) THE VERTICAL SCHOOL.

4. CONCLUSION

In this work, the traveling wave is imposed on a trout-like model to mimic trout swimming. A finite-difference-based sharp interface immersed boundary method is employed to simulate the swimming of minimal schools arranged in horizontal and vertical planes, including in-line, side-by-side, and vertical arrangements. The results show that the thrust and efficiency of the leading fish in the in-line school can be enhanced by 3.78% and 5.28%, respectively. In comparison, the swimming efficiency of the following fish reduces by 3.17% due to the significant increase in power consumption on the trunk. In the side-by-side school, even though the total thrust of the system only increases by 2.28%, the swimming efficiency is enhanced by 3.86% because the power consumption of the caudal decreases by 6.17%. Even though the swimming efficiency increases by less than 2% in the vertical school, the total thrust production is enhanced by 21.6%.

These results show that the drag and power consumption on the trout trunk can be easily disturbed by the flow and dramatically increases in these three schools. The side-by-side school can improve the swimming performance of individuals by reducing the power consumption on the caudal fins. In addition, the significant enhancement in thrust production of swimmers in the vertical school suggests the great potential of the hydrodynamic benefit in fish schools arranged in three-dimensional space.

ACKNOWLEDGEMENTS

This work is supported by NSF CNS grant no. CPS-1931929 and ONR MURI grant no. N0014-14-1-0533 and ASME FED GSS, and School of Engineering and Applied Science Distinguished Fellowship of the University of Virginia.

REFERENCES

[1] Cech, J. J., and Moyle, P. B., 2004, Fishes: an introduction to ichthyology, Pearson/B. Cummings.

- [2] Brock, V. E., and Riffenburgh, R. H., 1960, "Fish schooling: a possible factor in reducing predation," ICES Journal of Marine Science, 25(3), pp. 307-317.
- [3] Pitcher, T. J., 1986, "Functions of shoaling behaviour in teleosts," The behaviour of teleost fishes, Springer, pp. 294-337.
- [4] Herskin, J., and Steffensen, J. J. J. o. F. B., 1998, "Energy savings in sea bass swimming in a school: measurements of tail beat frequency and oxygen consumption at different swimming speeds," 53(2), pp. 366-376.
- [5] Killen, S. S., Marras, S., Steffensen, J. F., and McKenzie, D. J., 2012, "Aerobic capacity influences the spatial position of individuals within fish schools," Proceedings of the Royal Society B: Biological Sciences, 279(1727), pp. 357-364.
- [6] Weihs, D., 1973, "Hydromechanics of fish schooling," Nature, 241(5387), pp. 290-291.
- [7] Boschitsch, B. M., Dewey, P. A., and Smits, A. J., 2014, "Propulsive performance of unsteady tandem hydrofoils in an inline configuration," Physics of Fluids, 26(5).
- [8] Dewey, P. A., Quinn, D. B., Boschitsch, B. M., and Smits, A. J., 2014, "Propulsive performance of unsteady tandem hydrofoils in a side-by-side configuration," Physics of Fluids, 26(4).
- [9] Kurt, M., Eslam Panah, A., and Moored, K. W., 2020, "Flow Interactions Between Low Aspect Ratio Hydrofoils in In-line and Staggered Arrangements," Biomimetics, 5(2), p. 13.
- [10] Hemelrijk, C. K., Reid, D. A. P., Hildenbrandt, H., and Padding, J. T., 2015, "The increased efficiency of fish swimming in a school," Fish and Fisheries, 16(3), pp. 511-521.
- [11] Pan, Y., and Dong, H., 2020, "Computational analysis of hydrodynamic interactions in a high-density fish school," Physics of Fluids, 32(12), p. 121901.
- [12] Daghooghi, M., and Borazjani, I., 2015, "The hydrodynamic advantages of synchronized swimming in a rectangular pattern," Bioinspir Biomim, 10(5), p. 056018.
- [13] Verma, S., Novati, G., and Koumoutsakos, P., 2018, "Efficient collective swimming by harnessing vortices through deep reinforcement learning," Proc Natl Acad Sci U S A, 115(23), pp. 5849-5854.
- [14] Videler, J., and Hess, F., 1984, "Fast continuous swimming of two pelagic predators, saithe (Pollachius virens) and mackerel (Scomber scombrus): a kinematic analysis," Journal of experimental biology, 109(1), pp. 209-228.
- [15] Bozkurttas, M., Dong, H., Seshadri, V., Mittal, R., and Najjar, F., 2005, "Towards Numerical Simulation of Flapping Foils on Fixed Cartesian Grids," 43rd AIAA Aerospace Sciences Meeting and Exhibit.
- [16] Liu, G., Ren, Y., Dong, H., Akanyeti, O., Liao, J. C., and Lauder, G. V., 2017, "Computational analysis of vortex dynamics and performance enhancement due to body–fin and fin–fin interactions in fish-like locomotion," Journal of Fluid Mechanics, 829, pp. 65-88.
- [17] Pan, Y., Han, P., Huang, J., and Dong, H., 2020, "Effect of Formation Pattern on Schooling Energetics in Fish-Like Swimming," Fluids Engineering Division Summer Meeting, American Society of Mechanical Engineers, p. 003T005A046.

- [18] Pan, Y., Wang, J., and Dong, H., "Study on the passive pitching mechanism of different forms of flapping motion in turning flight," Proc. AIAA Aviation 2019 Forum, p. 3435.
- [19] Han, P., Pan, Y., Liu, G., and Dong, H., 2022, "Propulsive performance and vortex wakes of multiple tandem foils pitching in-line," Journal of Fluids and Structures, 108, p. 103422.
- [20] Wang, J., Ren, Y., Li, C., and Dong, H., 2019, "Computational investigation of wing-body interaction and its lift enhancement effect in hummingbird forward flight," Bioinspiration & biomimetics, 14(4), p. 046010.
- [21] Pan, Y., Zhang, Z., and Dong, H., "Computational study on the gliding flight of a damselfly," Proc. AIAA SCITECH 2022 Forum, p. 0728.
- [22] Zhang, W., Pan, Y., Gong, Y., Dong, H., and Xi, J., 2021, "A Versatile IBM-Based AMR Method for Studying Human Snoring," American Society of Mechanical Engineers, p. V001T002A039.
- [23] Koehler, C., Wischgoll, T., Dong, H., and Gaston, Z., 2011, "Vortex visualization in ultra low Reynolds number insect flight," IEEE transactions on visualization and computer graphics, 17(12), pp. 2071-2079